Int. J. Electrochem. Sci., 8 **(2013)** 1598 - 1608

International Journal of
ELECTROCHEMICAL
SCIENCE
www.electrochemsci.org

Sensitivity of encapsulated diamond-protein transistor renewed by low temperature hydrogen plasma

Marie Krátká[1*], *Neda Neykova*[1,2], *Egor Ukraintsev*[1], *Alexander Kromka*[1] *and Bohuslav Rezek*[1]

[1] Institute of Physics ASCR, Cukrovarnická 10, 162 00 Prague 6, Czech Republic
[2] Czech Technical University in Prague, Faculty of Nuclear Sciences and Physical Engineering, Trojanova 13, 120 00 Prague 2, Czech Republic
*E-mail: kratka@fzu.cz

Received: 31 July 2012 / *Accepted:* 29 October 2012 / *Published:* 1 February 2013

We study effects of low temperature hydrogen plasma treatment (200 – 300 °C) done in two different microwave plasma reactors (linear and focused plasma) on functionality of diamond solution-gated field-effect transistors (FET) covered with various encapsulation (ma-P, OFPR, SU8, Si_3N_4) and with proteins adsorbed on the gate. Three-dimensional transistor microstructures (20 μm) are made of nanocrystalline hydrogen terminated intrinsic diamond that is grown on Si/SiO_2 substrates by selective seeding and microwave plasma CVD growth. The hydrogen-plasma treatment in linear plasma system at 200 °C removes the proteins from the gate as evidenced by atomic force microscopy, keeps the FET fully operational, and renews solution-gated FET sensitivity to protein adsorption (unlike rinsing in solutions) as evidenced by reproducible shift of transfer characteristics by -30 mV. At the same time, due to larger distance (7 cm) from the high-density plasma region this process enables to preserve the polymer-based encapsulation, unlike to more aggressive treatment in focused plasma.

Keywords: Nanocrystalline Diamond; Solution-gated Field-effect Transistor; Low Temperature Hydrogen Termination; Proteins; Encapsulation

1. INTRODUCTION

Diamond exhibits unique combination of electrical, optical and mechanical properties with chemical and biocompatible properties [1,2] and it is a perspective material for bioelectronic and electrochemical applications [3]. Diamond films can be employed as biosensors such as catalytic glucose sensors [4], capacitive sensors [5] or solution-gated field-effect transistors (FET) [6,7] taking advantage of diamond unique chemical and electronic properties. In particular FET sensors enable

miniaturization and direct transduction of signals in biosensing. This is indispensable for high density, high sensitivity, and high-speed sensors [8,9]. Label-free FET biosensors demonstrated the ability to detect lower concentrations of molecules, such as prostate specific antigen [10].

The main advantages of diamond FETs in comparison to conventional silicon FETs are excellent diamond biocompatibility and operation without a gate oxide layer. The gate is insulated by hydrogen atoms hence it allows intimate contact between biomolecules and the surface of FET channel. Comparison of the solution-gated FETs with various grain sizes showed that electronic transport across grain boundaries is not influenced by protein adsorption. Thus only diamond grains themselves control the interaction of proteins with the surface conductive layer and resulting function of the FET devices based on H-terminated intrinsic NCD [11].

The diamond solution-gated FETs were at first used for *pH* [12,13] and DNA hybridization sensing [14]. Later on they were used for monitoring enzyme function and most recently for monitoring cell activity [7]. Thus understanding the role of proteins from cell medium on the FET response and renewal of the response is fundamental for such sensor applications.

The FET-based biosensors are often encapsulated by different types of photoresists which are relatively easy to prepare and remove. Silicon nitride can be also used for encapsulation [15] but such technology is more complicated and not so much available in the labs.

Common diamond solution-gated FETs based on hydrogen-terminated diamond surface conductivity are prepared by a number of diverse technological steps including photo-lithography, lift-off, selective oxidation, encapsulation, deposition of contacts etc. [6,11]. This is complicated for renewal of a sensor device because for instance proteins and other organic molecules are persistent on the surface [6]. It was shown by atomic force microscopy (AFM) that proteins in the cell growth medium create thin inter-layer on the diamond surface which remains even after phosphate buffered saline and water rinsing [16]. Typically one needs treatment in boiling acid for removing the protein layer. Such sample handling destroys C-H surface termination. Therefore, such H-terminated diamond solution-gated FETs must be fabricated by repeating all the technological steps.

A direct growth of nanocrystalline diamond (NCD) micro-structures via patterning of a nucleation/seeding layer can provide an alternative solution [17-19]. It was already demonstrated that directly grown nanocrystalline diamond FET micro-structures (average grain size 250 nm) are operational in both solid-state and solution-gated field-effect transistor configurations [18]. Further advantages of NCD comparison to monocrystalline diamond (MCD) are easy fabrication, possibility of deposition on large areas and on arbitrary substrates (silicon, glass [20], metals [21] and plastic [22]). NCD films are also much less expensive compared to MCD.

Therefore, here we employ solution-gated FETs based on directly grown NCD micro-channels (20 μm). We compare both organic resins and silicon nitride as encapsulation materials. We study if such complete encapsulated devices can be recycled after low temperature hydrogenation (LTH) [23] process via cleaning the gate surface from proteins and at the same time preserving H-termination of diamond surface. We characterize effects of low temperature hydrogen plasma treatment (200 – 300 °C) in two different microwave plasma reactors (linear and focused plasma) on diamond transistor characteristics and on etching of organic resin and silicon nitride encapsulation.

2. EXPERIMENTAL PART

2.1. Fabrication of directly grown NCD micro-channels

Direct growth of NCD channels was performed by microwave plasma chemical vapor deposition (CVD) on cleaned Si/SiO_2 substrates (10×10 mm^2, 1.5 μm thickness of SiO_2). Directly grown NCD FET channels were prepared by photolithographic processing with two polymer layers and by reactive ion etching (RIE) through photolithographic mask. The process is schematically shown in Fig. 1 and details can be found in the literature [24]. Briefly, Si/SiO_2 substrates were first covered with OFPR photoresist layer by spin-coating and dried at 100 °C (Fig. 1a). Then they were seeded with diamond nanoparticles applying an ultrasonic treatment (Fig. 1b). The seeding layer was covered by OFPR layer and dried (Fig. 1c). Thus diamond seeds are packed between two photosensitive layers (sandwich-like structure). This improves the pattern selectivity for diamond growth [24]. Microchannels were defined by photolithography patterning (Fig. 1d). Then, the reactive ion etching (CF_4/O_2 r.f. plasma parameters: 100 W, 150 mTorr, 3 min) was used as the final treatment step (Fig. 1e).

Afterwards, growth of NCD thin films was performed in a focused microwave plasma CVD system (AIXTRON P6) from a methane/hydrogen gas mixture (Fig. 1f). Process parameters were as follows: microwave power 2.5 kW, 1% methane in hydrogen, total gas pressure 50 mbar, substrate temperature 800 °C, and total growth time 3 h. The surfaces of resulting three-dimensional diamond micro-structures were hydrogen-terminated in pure hydrogen plasma at 600 °C for 10 min in the same microwave apparatus.

The structure and material composition of the directly grown H-NCD channels were studied by scanning electron microscopy (SEM), micro-Raman spectroscopy, and AFM using standard silicon cantilevers with a nominal tip radius of 10 nm.

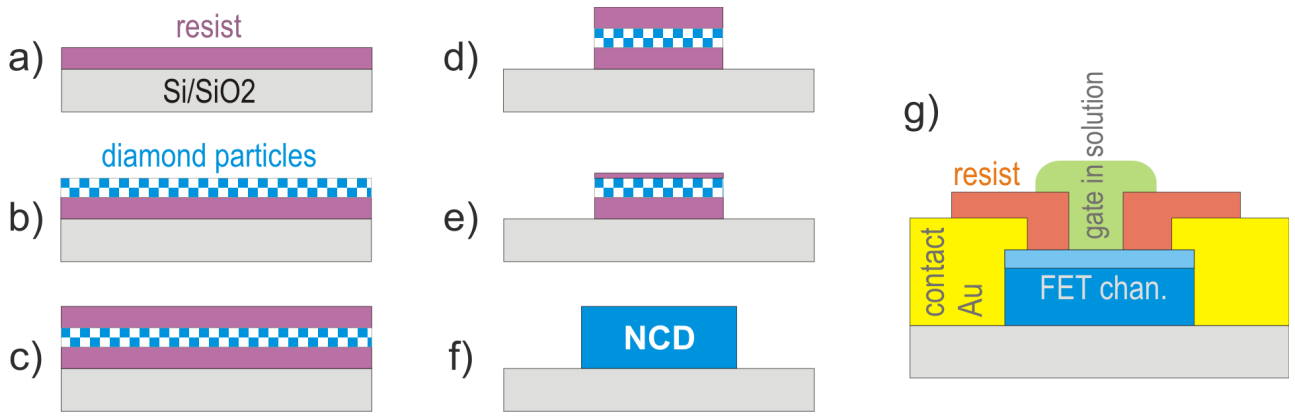

Figure 1. Schematic illustration of the processing steps for fabrication of NCD micro-channels: coating with one layer of photoresist (a), seed layer formation (b), coating with second layer of photoresist (c), photolithography patterning (d) etching using RIE (e) and final growth of NCD micro-channel (f). Scheme of the complete solution-gate FET device with surface conductive, H-terminated diamond channel (g).

2.2. Fabrication of solution-gated *FET devices*

For making complete FET device (see the scheme in Fig. 1g), source and drain contacts were prepared by thermal evaporation (10 nm of Ti and 50 nm of Au) through lithographic masks followed by lift-off technique. The mask was removed in acetone and photoresist stripper (remover mr-REM 660). Then the area between contacts was covered with different types of photoresists: positive photoresists OFPR (thickness 2 – 4 μm) and ma40 (4 μm) or with negative photoresist SU8 3010 (10 μm). Deep UV curing of the photoresist for hardening and biocompatibility was applied on positive photoresists. Photolithographic mask exposed openings of 60×60 μm^2 to define an active gate area (20 μm channel surrounded by 20 μm substrates areas in each side). For testing effects of LTH on different type of encapsulation we used also silicon nitride Si_3N_4 layers (thickness 150 nm). Si_3N_4 was deposited on silicon substrates from nitrogen and silane by plasma enhanced CVD. Profilometer measurements were used to determine thickness of all encapsulating materials before and after LTH treatment. Polymer etching rates were calculated from the thickness difference and process time.

2.3. Transistor characteristics setup

The transistor characteristics were measured using Keithley K327 source-measure units. The characteristics were measured in amplification regime at U_{ds} = -0.6 V in buffer solutions. Gating of FET was realized by immersing H-terminated channel into electrolyte solutions which were in contact with Ag/AgCl gate electrode. Types of used solutions were: (1) heat inactivated 15% fetal bovine serum (FBS; Biowest) and HEPES, (2) HEPES buffer alone. It is possible to measure diamond FETs in various electrolytes and buffer solutions [12,14]. We chose the HEPES buffer solution because it is typically used in experiments with cells [6,11]. We show always the fifth characteristic, which is stabilized in short term. The sweeping rate was 50 mV/s and initial delay time was 5 s. All experiments were performed at room temperature. We used a self-made measurement software that was built upon a measurement and control software package developed under Delphi by A. Fejfar, Institute of Physics.

2.4. Low temperature hydrogenation setup

Commonly used relatively high substrate temperatures (T ≥ 600 °C) during diamond growth and hydrogenation lead to partial or complete damage of the metal electrodes or other electronic parts [25]. Thus, 3D transistors including the encapsulation (resist OFPR, ma40, SU8 3010), gold contacts and with adsorbed proteins on diamond surface were exposed to hydrogen plasma using low temperature in two microwave plasma reactors (focused plasma reactor and linear plasma reactor). Fig. 2 shows a schematic drawing of fundamental differences between these two reactor setups. The main advantage of LTH in linear plasma reactor is a larger distance (7 cm) between the high-density plasma region and the sample surface [23,26]. Hydrogen termination at 200 °C performed in linear antenna plasma system is efficient to induce hydrogen-terminated conductive surfaces. No damage of polymer-based passivating layer (SU8) as well as Au contacts was observed [23]. In our case samples were

exposed to linear hydrogen plasma at the following conditions: microwave power 1000 W, vacuum pressure 0.3 mbar, 100 sccm of hydrogen flow, and processing time 30 min. The substrate temperature was in the range of 200 – 300 °C with the accuracy of ±10 °C.

The parameters of LTH in focused plasma were as follows: microwave power 800 – 1500 W, vacuum pressure 20 – 30 mbar, hydrogen flow 300 sccm, temperature 300 °C (the lowest achievable), processing time 20 min.

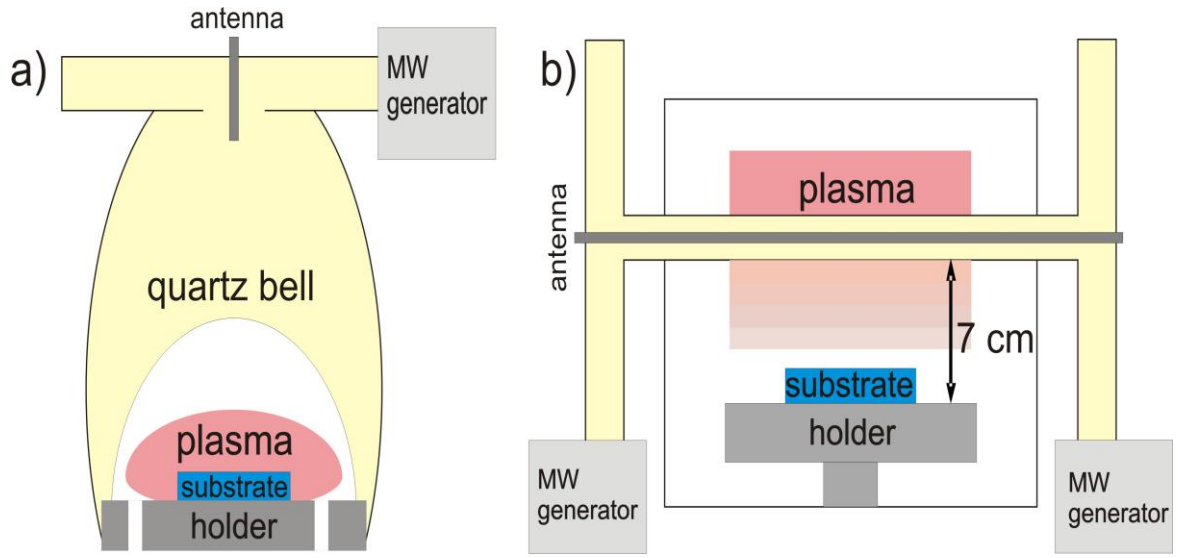

Figure 2. Schematic drawing of microwave CVD reactors: focused plasma reactor (a) and linear antenna reactor (b). Position of the substrate with respectg to the plasma is indicated.

2.5. AFM study of protein layer

Study of protein layer was performed using AFM on monocrystalline diamond. In AFM experiments polished MCD substrates with RMS roughness < 1 nm were used instead of NCD substrates with RMS roughness > 10 nm. Low substrate roughness is required for such measurements because the thickness of protein layer is around 2 – 4 nm. Moreover, it is hard to detect FBS layer on NCD by AFM due to high tip wear during AFM nanoshaving. For those measurements the Ntegra AFM (NT-MDT) with Multi75Al cantilevers (Budget sensors) was used. To analyze AFM results Nova (NT-MDT) and Gwyddion software were used.

To check the effectiveness of low temperature hydrogen termination, FBS was adsorbed on the surface of MCD from 15% FBS solution for 10 min. Then the sample was cleaned with water and dried by air flow. The thickness of the protein layer was measured in air using AFM nanoshaving method [27-29]. Then the low temperature hydrogen termination at 200 °C was performed and the protein thickness was again measured using the same method.

3. RESULTS AND DISCUSSION

The SEM image of directly grown NCD micro-channels with the channel width of 20 μm is shown in Fig. 3a. It is noticeable that the employed fabrication process of NCD channels leads to a very good selectivity of diamond structure formation [24]. The average grain size is 250 nm as estimated from the detailed SEM image in Fig. 3b. The NCD grains have clear crystal shapes with flat facets with some dislocations and thin grain boundaries. This good crystalline diamond character of the microstructures is corroborated by micro-Raman spectrum in Fig. 3d. The Raman spectrum exhibits characteristic sharp diamond peak at 1332 cm^{-1} and some graphitic phase (broad G-band at 1580 cm^{-1}) whcih is related with the grain boundaries. Fig. 3d shows a three-dimensional AFM image of the directly grown NCD micro-channel. Thickness of the diamond structure, calculated from the AFM height histogram, was 650 nm.

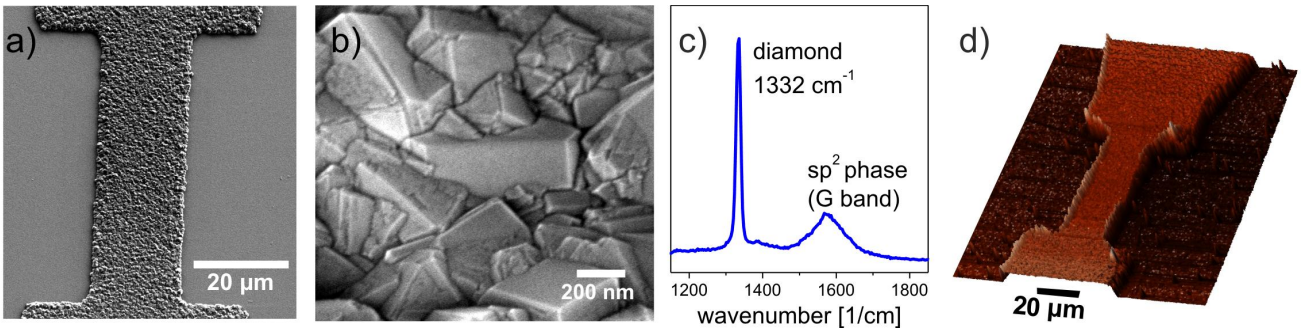

Figure 3. SEM image (a), detailed SEM morphology (b), micro-Raman spectrum (c), and AFM morphology (d) of a directly grown NCD micro-channel.

We observed that application of FBS to the solution-gated FET decreased the FET conductivity as reflected by the shift of transfer characteristics by -30 mV and by the decreased slope (transconductance) as shown in Fig. 4. This shift is permanent even after rinsing the FET in diverse solutions (deionized water, phosphate buffered saline or other agents; Fig. 4). This is in full agreement with our results on conventional planar solution-gated FETs [6,11] where we attributed this shift to the adsorption of a 2–4 nm primary protein layer from FBS. This protein layer remains on diamond irrespective of rinsing [16,28] and modifies original equilibrium of the surface conductive layer system by replacing ions in the very vicinity of the diamond surface like in the case of DNA molecules or lipid bilayers [30,31]. All the characteristics show some hysteresis. It is obtained by sweeping U_g from positive to negative values and back. This behavior is typical for solution-gate FET. It is not observed for solid gate (Al) on the same material. Thus it is related with the capacitive response of the diamond-electrolyte interface. The magnified plot shows the transconductance characteristics for only one sweep direction (indicated by the arrow) for better clarity, thus there is no hysteresis visible.

After the FET characteristic measurements the samples were recycled by the LTH. Fig. 5 shows AFM images of diamond surface and protein layer before and after low-temperature hydrogenation. By using the AFM nanoshaving method, Fig. 5b evidences the presence of such protein layer also here, compared to the initial surface. Moreover, Fig. 5c shows that the low temperature

hydrogen termination in linear antenna plasma (at 200 °C) successfully removed this FBS protein layer from the monocrystalline diamond surface (unlike rinsing in the solutions). Only < 1 nm thin layer (probably some residual hydrocarbons from the plasma process) remains on the surface which should be taken into account in further experiments.

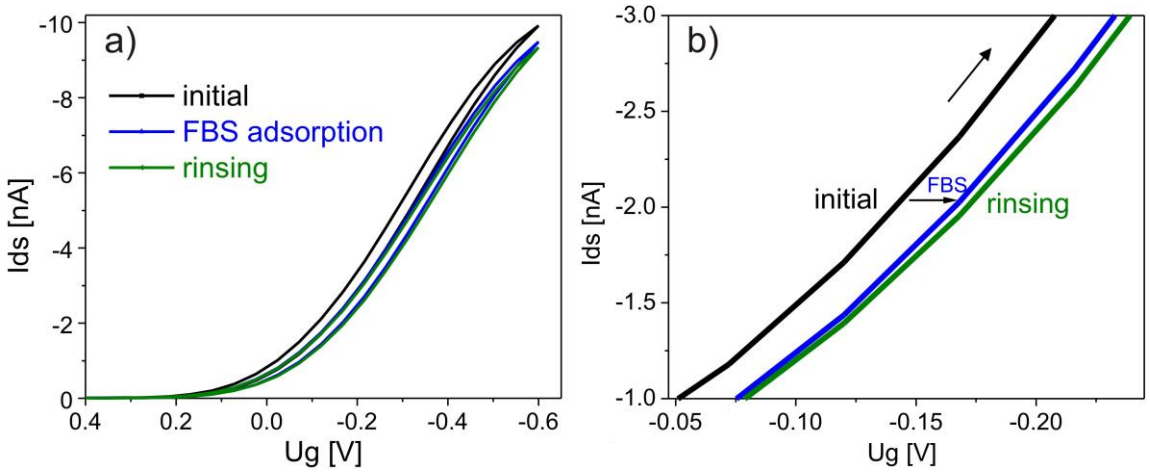

Figure 4. Transistor transfer characteristics measured in HEPES buffer solution at U_{ds} = -0.6 V (initial – black curve; after FBS adsorption – blue; after rinsing – green) (a). Magnified part of the transconductance characteristics showing FET response for one U_g sweep direction (indicated by the arrow) (b).

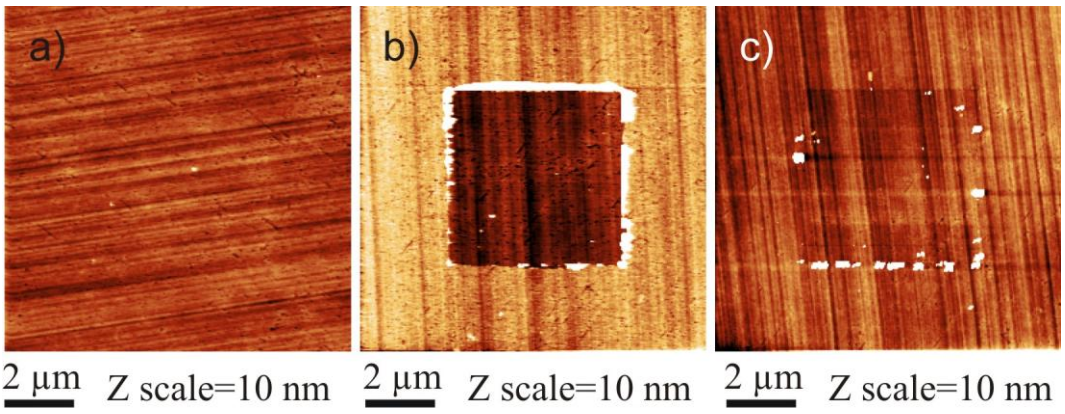

Figure 5. AFM characterization of diamond surface (a) and protein layer before (b) and after low-T hydrogenation (c).

The transistor currents after LTH are generally about 5 times lower compared to the currents after standard hydrogenation at 600 °C in the focused plasma system [11,32]. Nevertheless, the Fig. 6 evidences that the directly grown FETs are still fully operational after LTH at 200 °C in linear plasma reactor even after repeated LTH process. This is in agreement with the study of hydrogen termination performed in linear antenna plasma system which was shown to be efficient enough to generate conductive hydrogen-terminated surfaces at 200 °C. However, an increase in the substrate temperature up to 400 °C resulted in further increase in the surface conductivity [23]. The hydrogenation process is

thus less efficient due to lower temperature as well as due to lower plasma density in the linear antenna reactor. On the other hand, the encapsulation is preserved because of that and surface conductivity and sensor response is still achieved.

When the LTH was repeated on the same device we observed fluctuations of threshold voltage U_t within about 150 mV (Fig. 6b). Transconductances (slope of I_{ds} (U_g)) calculated at I_{ds} in the linear region of transfer characteristics are 10.5 nS and 11 nS at U_{ds} = −0.6 V, I_{ds} = −2.0 nA for transfer characteristics after first and second LTH process, respectively. Thus transconductance remained similar. This indicates that the fluctuations are related to the variation of gate potential but not to the equilibrium of surface conductive layer. This is unlike the case when proteins were adsorbed on the surface [6]. On the other hand, it is in a good agreement with the fact that transistors characteristics were measured in buffer solution which should maintain stable surface conditions. Origin of these U_t fluctuations is still unknown. Fluctuations after standard hydrogen termination (600 °C) as well as after LTH in focused plasma can not be investigated because covering resists are removed during these processes and thus transistor characteristics can not be measured.

Applying FBS proteins on diamond solution-gated FET after repeated LTH process at 200 °C caused the same shift of transfer characteristic (-30 mV) like in the case of FBS adsorption on initial diamond FET (Fig. 6b). Thus, sensitivity of encapsulated diamond-protein transistor is renewed by low temperature hydrogen plasma. It may be noted that we observed only a negligible change of transconductance after the repeated LTH and protein adsorption. We speculate that this may be due to the remaining sub-nm contamination layer observed by AFM in Fig. 5c.

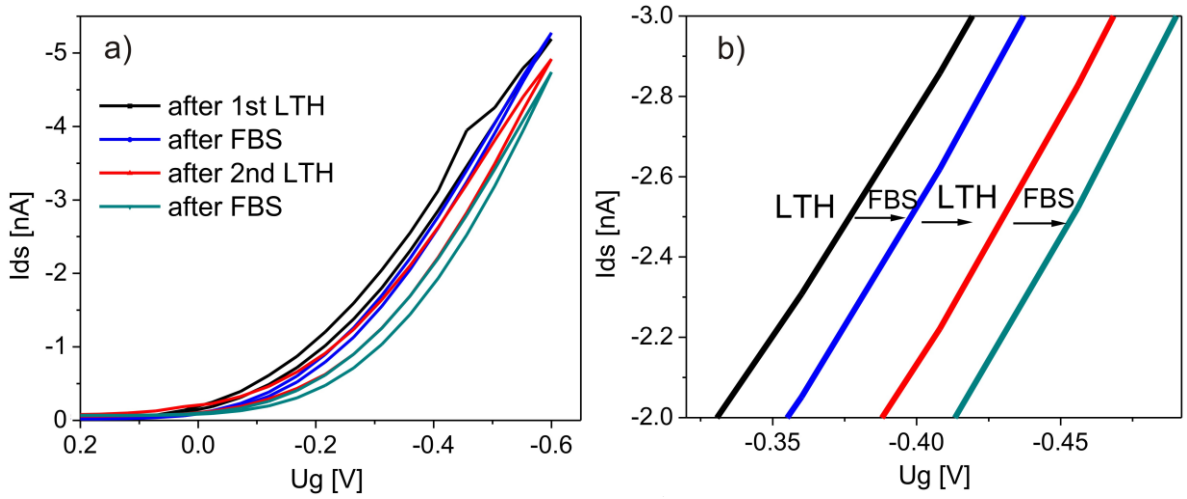

Figure 6. Transistor characteristics after repeated LTH process in linear plasma at 200 °C and after FBS adsorption (a) and magnified part of the transconductance characteristics showing FET response for one U_g sweep direction (b). All transfer characteristics were measured in HEPES at U_{ds} = -0.6 V.

Fig. 7 shows etching rates after LTH for different types of encapsulation and temperatures. All the data are related to linear plasma except for SU8 3010 and for Si_3N_4 (“stars”) which have been

obtained after LTH in the focused plasma at 300 °C. If the resins where fully removed after the LTH process, the etching rates were determined as bottom estimates based on the initial resin thickness.

LTH in the linear plasma is less aggressive to encapsulation than focused plasma most likely due to larger distance (7 cm) between the high density plasma region and the sample surface [23,26]. In the focused plasma the sample is in or in the very vicinity of plasma ball. We observed increased etching rates (from 3 to 400 nm/min for photoresists and from 0 to 1.5 nm/min for Si_3N_4) as a function of hydrogenation temperature (200 – 300 °C). Based on the data of LTH in the linear plasma, photoresist SU8 is the most stable of the employed organic resins and it can be used up to 300 °C. Photoresist OFPR is removed during LTH process in linear plasma at the temperature about 260 °C and its quality remains good up to this temperature. Photoresist ma40 appears as the least stable, having bad quality (cracks and bubbles) already at 200 °C. Silicon nitride is the most resistant from the employed materials for encapsulation. Its etching rate after LTH in the linear plasma is in the range of 0 to 0.2 nm/min as a function of hydrogenation temperature and 1.5 nm/min in the focused plasma at 300 °C. Thus silicon nitride is the most robust yet difficult to employ encapsulation. As for gold contacts, their quality appears good even after LTH in the focused plasma.

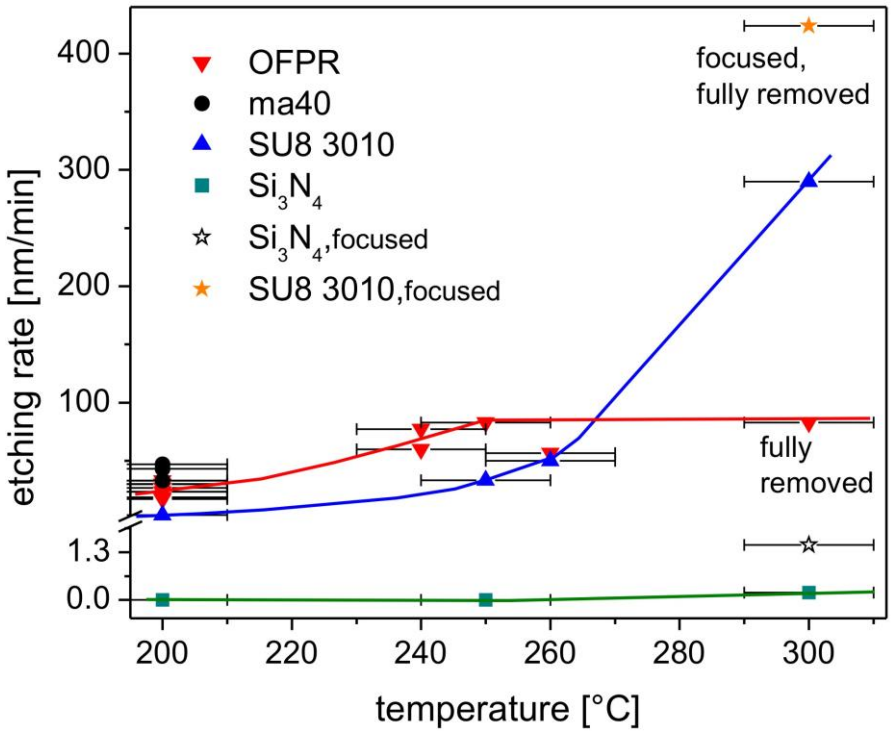

Figure 7. Etching rates for photoresists (OFPR, ma40 and SU8 3010) and for silicon nitride as a function of temperature.

4. CONCLUSIONS

We showed that the low temperature hydrogen plasma treatment of NCD solution-gated FET devices in linear plasma system is less aggressive on encapsulation than focused plasma due to larger

distance between the high-density plasma region and the sample surface. It kept the similar electronic quality (yet reduced thickness) of covering encapsulation and gold contacts. It successfully removed FBS proteins from the diamond surface. The transistor currents were lower (about five times) after this treatment compared to the focused plasma performed at standard temperature of hydrogenation (600 °C). When the LTH process was repeated on the same device we observed fluctuations of the threshold voltage U_t within about 150 mV. Origin of these U_t fluctuations is still unknown. Yet, diamond solution-gated FETs were fully operational after this treatment and the sensitivity to protein adsorption was renewed. Therefore, the directly grown three-dimensional diamond transistors including the encapsulation and gold contacts can be recycled by low temperature hydrogenation in linear antenna reactor within 30 minutes without any further processing.

ACKNOWLEDGEMENTS

Technical support of Jitka Libertínová, Oleg Babchenko, Martin Ledinský, Jiří Stuchlík, Zdeňka Poláčková, Karel Hruška, Vlastimil Jurka, Antonín Fejfar, Antonín Brož and Marie Kalbacova is gratefully appreciated. This research was financially supported by the projects P108/12/0996 (GACR), P108/12/G108 (GACR), doctoral project 202/09/H041, SVV-2012-265304 and by the Fellowship J.E. Purkyně (AK). The work occurred in frame of LNSM infrastructure.

References

1. L. Tang, C. Tsai, W. Gerberich, L. Kruckeberg and D. Kania, *Biomaterials,* 16 (1995) 483
2. M. Kalbacova, M. Kalbac, L. Dunsch, A. Kromka, M. Vaněček, B. Rezek, U. Hempel and S. Kmoch, *phys. stat. sol. (b),* 244 (2007) 4356
3. A. Kraft, *Int. J. Electrochem. Sci.,* 2 (2007) 355
4. K. E. Toghill and R. G. Compton, *Int. J. Electrochem. Sci.,* 5 (2010) 1246
5. M. H. Abouzar, A. Poghossian, A. Razavi, A. Besmehn, N. Bijnens, O. A. Williams, P. Wagner and M. J. Schöning, *phys. stat. sol. (a),* 205, (2008) 2141
6. B. Rezek, M. Krátká, A. Kromka and M. Kalbacova, *Biosens. Bioelectron.,* 26 (2010) 1307
7. M. Dankerl, S. Eick, B. Hofmann, S. Ingebrandt, A. Offenhäusser, M. Stutzmann and J. A. Garrido, *Adv. Funct. Mater.,* 19 (2009) 2915
8. K.-S. Song, T. Hikari, H. Umezawa and H. Kawarada, *Appl. Phys. Lett.,* 90 (2007) 063901
9. S. Ingebrandt, Y. Han, F. Nakamura, A. Poghossian, M. Schöning and A. Offenhäusser, *Biosens. Bioelectron.,* 22 (2007) 2834.
10. Chi-Chang Wu, Tung-Ming Pan, Chung-Shu Wu, Li-Chen Yen, Cheng-Keng Chuang, See-Tong Pang, Yuh-Shyong Yang and Fu-Hsiang Ko, *Int. J. Electrochem. Sci.,* 7 (2012) 4432
11. M. Krátká, A. Kromka, E. Ukraintsev, M. Ledinský, A. Brož, M. Kalbacova and B. Rezek, *Sens. Actuators B,* 166-167 (2012) 239
12. C.E. Nebel, B. Rezek, D. Shin, H. Watanabe and T. Yamamoto, *J. Appl. Phys.,* 99 (2006) 033711
13. M. Dankerl, A. Reitinger, M. Stutzmann and J.A. Garrido, *phys. stat. sol. Rapid Res. Lett.*. 2 (2008) 31
14. K.-S. Song, G.-J. Zhang, Y. Nakamura, K. Furukawa, T. Hiraki, J.-H. Yang, T. Funatsu, I. Ohdomari and H. Kawarada, *Phys. Rev. E* ,74 (2006) 041919
15. T. Sakata, M. Kamahori and Y. Miyahara, *Materials Science and Engineering: C,* 24 (2004) 827
16. B. Rezek, E. Ukraintsev, L. Michalíková, A. Kromka, J. Zemek and M. Kalbacova, *Diam. Relat. Mater.,* 18 (2009) 918

17. A. Kromka, O. Babchenko, B. Rezek, M. Ledinský, K. Hruška, J. Potměšil and M. Vaněček, *Thin Solid Films,* 518 (2009) 343
18. H. Kozak, A. Kromka, O. Babchenko and B. Rezek, *Sensor Lett.,* 8 (2010) 482
19. O. Babchenko, E. Verveniotis, K. Hruska, M. Ledinsky, A. Kromka and B. Rezek, *Vacuum,* 86 (2012) 693
20. A. Kromka, B. Rezek, Z. Remeš, M. Michalka, M. Ledinský, J. Zemek, J. Potměšil and M. Vaněček, *Chem. Vap. Deposition,* 14 (2008) 181
21. J. Čermák, A. Kromka and B. Rezek, *phys. stat. sol. (a),* 205 (2008) 2136
22. A. Kromka, O. Babchenko, H. Kozak, B. Rezek and M. Vanecek, *phys. stat. sol. (b),* 246 (2009) 2654
23. N. Neykova, H. Kozak, M. Ledinsky and A. Kromka, *Vacuum,* 86 (2012) 603
24. O. Babchenko, T. Izak, E. Ukraintsev, K. Hruska, B. Rezek and A. Kromka, *phys. stat. sol. (b),* 247 (2010) 3026
25. N. Neykova, O. Babchenko, H. Kozak, A. Kromka, K. Hruška and M.Vaněček, *15th International Conference on Applied Physics of Condensed Matter, Bystra, Liptovsky Jan, Slovak Republic,* ISBN 978-80-554-0057-0 (2009), 256
26. A. Kromka, O. Babchenko, T. Izak, K. Hruska and B. Rezek, *Vacuum,* 86 (2012) 776
27. B. Rezek, L. Michalíková, E. Ukraintsev, A. Kromka and M. Kalbacova, *Sensors,* 9 (2009) 3549
28. E. Ukraintsev, B. Rezek, A. Kromka, A. Broz and M. Kalbacova, *phys. stat. sol. (b),* 246 (2009) 2832
29. B. Rezek, D. Shin, H. Uetsuka and C. E. Nebel, *phys. stat. sol. (a),* 204 (2007) 2888
30. A. Poghossian, A. Cherstvy, S. Ingebrandt, A. Offenhäusser and M. Schöning, *Sens. Actuators B,* 111–112 (2005) 470
31. P. K. Ang, K. P. Loh, T. Wohland, M. Nesladek and E. Hove, *Adv. Funct. Mater. 19,* (2009) 109
32. M. Krátká, N. Neykova, A. Kromka and B. Rezek, *Proc. of the 20th Annual Conference of Doctoral Students,* (2012) in press